# RSC Advances



This is an *Accepted Manuscript*, which has been through the Royal Society of Chemistry peer review process and has been accepted for publication.

Accepted Manuscripts are published online shortly after acceptance, before technical editing, formatting and proof reading. Using this free service, authors can make their results available to the community, in citable form, before we publish the edited article. This Accepted Manuscript will be replaced by the edited, formatted and paginated article as soon as this is available.

You can find more information about *Accepted Manuscripts* in the **Information for Authors**.

Please note that technical editing may introduce minor changes to the text and/or graphics, which may alter content. The journal's standard <u>Terms & Conditions</u> and the <u>Ethical guidelines</u> still apply. In no event shall the Royal Society of Chemistry be held responsible for any errors or omissions in this *Accepted Manuscript* or any consequences arising from the use of any information it contains.





# **Journal Name**

# **ARTICLE**

Received 00th January 20xx,

Accepted 00th January 20xx
DOI: 10.1039/x0xx00000x

www.rsc.org/

# Microstructure, mechanical properties and oxidation resistance of $SiC_f/SiC$ composites incorporated with boron nitride nanotubes

Guangxiang Zhu, abc Shaoming Dong, ab Dewei Ni, b Chengying Xu and Dengke Wang

SiC<sub>t</sub>/BNNTs-SiC hierarchical composites were fabricated via firstly in situ growth of boron nitride nanotubes (BNNTs) on the surface of silicon carbide (SiC) fibers using boron powder as raw material and subsequently matrix densification by chemical vapor infiltration (CVI) and polymer impregnation/pyrolysis (PIP) methods. With the incorporation of BNNTs, energy dissipation mechanisms at nanoscale triggered by BNNTs such as pullout, debonding, crack deflection and crack bridging are observed. But the positive effect of BNNTs on mechanical properties has not been raised due to the offset from the negative effect of pores in composites. Additionally, the residual boron powder results in an improved oxidation resistance and parabolic oxidation kinetics of  $SiC_f/SiC$  composites at  $900^{\circ}C$ , thanks to the protective effect of  $B_2O_3$  glassy phase formed by oxidation of boron. Consequently, a better strength retention after oxidation is obtained. Moreover, it is believed that the remained strengthening and toughening mechanisms aroused by BNNTs surviving after oxidation probably also make a contribution to the better strength retention.

# Introduction

Continuous silicon carbide (SiC) fiber reinforced SiC matrix (SiC<sub>f</sub>/SiC) composites have been universally used in aeroengine hot section components including exhaust cone, flame stabilizer, nozzle flap etc. due to their excellent properties, such as outstanding high-temperature strength, high fracture toughness, good thermal stability and low density. 1-3 By embedding continuous SiC fibers in the monolithic SiC ceramic matrix, energy dissipation mechanisms can be triggered including debonding at fiber/matrix interface, crack deflection, fiber bridging, sliding and pullout and so on, which ensures that SiC<sub>f</sub>/SiC composites exhibit a non-catastrophic failure mode.<sup>3</sup> Nonetheless, these energy dissipation mechanisms merely originate from micron scale fibers. The matrix at micron scale among fibers cannot be strengthened and toughened by the above-mentioned mechanisms, thus still showing a brittle behavior. Such matrix at micron scale are weak points in SiC<sub>f</sub>/SiC composites, of which the mechanical properties remain to be further improved.

In recent years, the development of one dimensional (1D) nanoscale reinforcements with extraordinary mechanical properties such as carbon nanotubes (CNTs) offers an effective

As a new kind of advanced 1D nanomaterial, boron nitride nanotubes (BNNTs) have drawn tremendous attention from scientists recently by virtue of their remarkable properties.  $^{11}$  On account of structural similarity to CNTs, BNNTs also present excellent properties such as high elastic modulus, high tensile strength and high thermal conductivity,  $^{11\cdot13}$  which endows BNNTs a potential application in composites as nanoscale reinforcements like CNTs. Moreover, BNNTs show much higher thermal and chemical stability than CNTs and possess good oxidation resistance up to 900  $^{\circ}\mathrm{C}$ .  $^{10,14}$  This superiority,

approach to solve the above-mentioned problem. 1D nanoscale reinforcements can be introduced into the matrix at micron scale among micron-diameter fibers.4 The existence of nanoscale reinforcements are expected to arouse additional energy dissipation mechanisms at nanoscale and improve the mechanical properties of matrix at micron scale. To avoid the agglomeration of nanostructures in matrix resulting from directly dispersion in the precursor, 4,5 in situ growing nanostructures directly on the surface of conventional microscale fibers to build fiber/nanostructures hierarchical (or multiscale or hybrid) structures is a favorable method to introduce nanoscale reinforcements into matrix of composites. And then. hierarchical composites are fabricated by depositing matrix into fiber/nanostructures hierarchical structures. To date, many researchers have reported fiber/CNTs hierarchical composites with remarkably improved mechanical properties by CNTs.<sup>5-9</sup> However, CNTs exhibit relatively poor oxidation resistance and readily oxidize in air above 400 °C, 10 thus leading to partial or total malfunction of strengthening and toughening mechanisms ascribed to CNTs and limiting their further applications at high temperatures.

<sup>&</sup>lt;sup>a</sup> State Key Laboratory of High Performance Ceramics and Superfine Microstructure, Shanghai Institute of Ceramics, Chinese Academy of Sciences, Shanghai 200050, China. E-mail address: composites@mail.sic.ac.cn; Tel: 0086-21-52414324 (S. Dong)

<sup>&</sup>lt;sup>b.</sup> Structural Ceramics and Composites Engineering Research Center, Shanghai Institute of Ceramics, Chinese Academy of Sciences, Shanghai 200050, China

<sup>&</sup>lt;sup>c</sup>. University of Chinese Academy of Sciences, Beijing 100049, China

<sup>&</sup>lt;sup>d.</sup> Department of Mechanical Engineering, Florida State University, Tallahassee, FL 32310 LISA

therefore, makes BNNTs more suitable than CNTs as nanoscale reinforcements in hierarchical composites for enduring service at high temperature in oxidizing environment. However, to the best of our knowledge, until now, almost no studies have been reported on the subject of fiber/BNNTs hierarchical composites.

In the present study, we report, for the first time, the fabrication of SiC fiber/BNNTs hierarchical reinforced SiC matrix composites (SiC<sub>f</sub>/BNNTs-SiC) by two steps: firstly in situ growth of BNNTs on the surface of SiC fibers to build fiber/BNNTs hierarchical structures, which has been reported in our previous work, 15 and subsequently matrix densification of hierarchical structures via chemical vapor infiltration (CVI) and polymer impregnation/pyrolysis (PIP) methods. In this paper, boron powder was employed as boron source for the growth of BNNTs. Moreover, it is anticipated that the residual part of boron powder after the growth of BNNTs can also serve as boron-bearing species that self-healing composites usually contain. The boron-bearing species can easily oxidize to form glassy phase (B<sub>2</sub>O<sub>3</sub>) to seal the cracks or pores and hinder the in-depth diffusion of oxygen, thus giving rise to improved oxidation resistance at relatively low temperatures (500-1000  $^{\circ}$ C).  $^{2,16}$  To confirm the existence of BNNTs in SiC<sub>f</sub>/SiC composites, the morphology, microstructure and chemical composition of nanoscale reinforcements were studied and discussed in this paper. What's more, microstructure, mechanical properties and oxidation resistance of SiC<sub>f</sub>/BNNTs-SiC hierarchical composites were investigated systematically.

### **Experimental**

#### Synthetic procedures

The fabrication of SiC<sub>f</sub>/BNNTs-SiC hierarchical composites was carried out by two steps: (1) At first, in order to build SiC<sub>f</sub>/BNNTs hierarchical structures, BNNTs were in situ grown on the surface of SiC fibers via a simplified ball milling, impregnation and annealing method using boron powder as raw material, as reported in our previous work. 15 Herein, SiC fiber (with an impurity element of oxygen: about 2.5 wt%) cloths (0/90°) with a size of 7cm x 7cm were adopted for the synthesis of SiC<sub>f</sub>/BNNTs hierarchical structures. Additionally, previous to in situ growth of BNNTs, pyrolytic carbon/silicon carbide multilayered interphases  $(PyC/SiC)_n$  (n=3) were deposited on SiC fiber cloths. PyC interphase accounts for about 7 wt% of the fiber colths. (2) Subsequently, CVI and PIP methods were employed to introduce the SiC matrix into the SiC<sub>f</sub>/BNNTs hierarchical structures. The fiber clothes with BNNTs in situ grown were stacked, and compressed together with a volume fraction of fibers of about 40%. Then those stacked fiber clothes were put into the CVI furnace and the SiC matrix was deposited into SiC<sub>f</sub>/BNNTs hierarchical structures at the temperature of 1000°C using methyltrichlorosilane (MTS, CH<sub>3</sub>SiCl<sub>3</sub>) and hydrogen (H<sub>2</sub>) as the precursors with the molar ratio of H2 to MTS of 10. The CVI process was repeated for several cycles. Then some relatively large pores failing to be fully occupied with matrix during the CVI process were further densified via PIP method, in which polycarbosilane (PCS) was employed as the precursor of SiC matrix and pyrolyzed at 900  $^{\circ}\mathrm{C}$  in argon (Ar) atmosphere. Finally, the relatively dense SiC<sub>f</sub>/BNNTs-SiC hierarchical composites were achieved. SiC<sub>f</sub>/SiC composites without BNNTs were fabricated via the same CVI and PIP process as described above for comparison.

#### Characterization

To investigate the oxidation resistance of composites, static oxidation test was carried out in a muffle furnace in static air at  $900\,^{\circ}\mathrm{C}$  for 40 h. The specimens were put into the furnace when the furnace was heated up to the desired temperature. Weight changes of the specimens were measured by an analytical balance with a sensitivity of  $\pm 0.01$  mg. Bulk density and open porosity of the composites were measured by Archimedes method. Flexural strength of the composites before and after oxidation was evaluated by a three-point bending test with a span of 30mm at a cross head speed of 0.5 mm/min on bar specimens with the dimension of  $2.9\text{mm}\times5.0\text{mm}\times45\text{mm}$ . The flexure strength value  $(\sigma_f)$  was determined by eqn(1):

$$\sigma_f = 3FL/(2bd^2) \tag{1}$$

where F, L, b and d are the load at the fracture point, the span length, the sample width and the sample thickness, respectively. In addition, fracture toughness was measured using single edge notched beam (SENB) method with a span of 30mm on bar specimens with the dimension of  $2.9 \text{mm} \times 5.0 \text{mm} \times 45 \text{mm}$  (with a notch of 2.5 mm in depth). The fracture toughness value ( $K_{IC}$ ) was calculated by eqn(2):

$$K_{IC} = (3pI/(2bw^{3/2}))[1.93-3.07(a/w)+1.45(a/w)^2-25.07(a/w)^3+25.8(a/w)^4]$$
 (2)

where p is the breaking load, I is the span length, b is the sample thickness, w is the sample width and a is the notch depth. The above mechanical properties measurements were carried out on an Instron-5566 universal testing machine. A small piece of the fiber cloth with BNNTs grown was used for the morphology characterization of BNNTs via a Hitachi SU8220 field-emission scanning electron microscopy (FESEM). To investigate the microstructure of the composites, the polished cross-sections and fracture surfaces of the composites were studied by FESEM. A JEM-2100F field emission transmission electron microscopy (FETEM) was used to characterize the microstructure of BNNTs. For microstructure analysis of BNNTs, a piece of the fiber cloth with BNNTs grown was ultrasonically vibrated in ethanol for 1-2h to collect adequate quantity of BNNTs from fibers first. Then the dispersion solution was dripped onto copper grids with a holey carbon film for TEM investigations. An x-ray energy dispersive spectroscopy (EDS) attached to FETEM was employed to determine chemical composition of BNNTs. The distributions of different elements in the polished crosssections of the composites after oxidation were investigated via an x-ray EDS attached to FESEM.

#### **Results and discussion**

A simplified ball milling, impregnation and annealing method was employed to in situ grow BNNTs on the surface of SiC fibers. The morphology, microstructure and chemical composition of as-grown BNNTs were exhibited in Fig. 1. It can be seen that the surface of fiber cloth is utterly encompassed by BNNTs, obscuring individual fiber within the cloth, as displayed in Fig. 1a-c. As-grown BNNTs have a length of around several tens of micrometers and entangle with each other, appearing to form a thick blanket besieging fibers. As estimated according to the weight change of fiber cloth before and after the growth of BNNTs, as-grown BNNTs account for about 2 wt% of the fiber cloth. The typical TEM images in Fig. 1d and e obviously reveal that BNNTs exhibit a multi-walled and bamboo-like structure with the average diameter of 30-160nm. Additionally, almost all the BNNTs apparently possess the bubble-chain walls, as indicated in Fig. 1d and e. The formation mechanism of bamboo-like BNNTs with bubblechain walls can be well explained with stress-induced sequential growth mode in vapor-liquid-solid (VLS) mechanism, as elaborately discussed in our previous work.<sup>15</sup> From the inset in Fig.1e, it can be illustrated that the nanotube has perfect crystalline structure with clear parallel fringes. The spacing between the parallel fringes is ~0.335nm, which is in line with  $d_{002}$  inter-planar distance of bulk h-BN. The EDS spectra of the nanotubes shown in Fig. 1f confirms that the nanotubes are BNNTs according to the strong B and N peaks. The Fe element is attributable to the steel particles which are introduced by ball-milling treatment with stainless steel balls and act as the catalysts for BNNTs growth. The Cu peak derives from the copper TEM grid and O element may be ascribed to the surrounding air absorbed on the surface of nanotubes. 15 These nanoscale "filaments", i.e. BNNTs, are incorporated with micro-scale SiC fibers to form hierarchical structures, which are used to fabricate SiC<sub>f</sub>/BNNTs-SiC hierarchical composites subsequently.

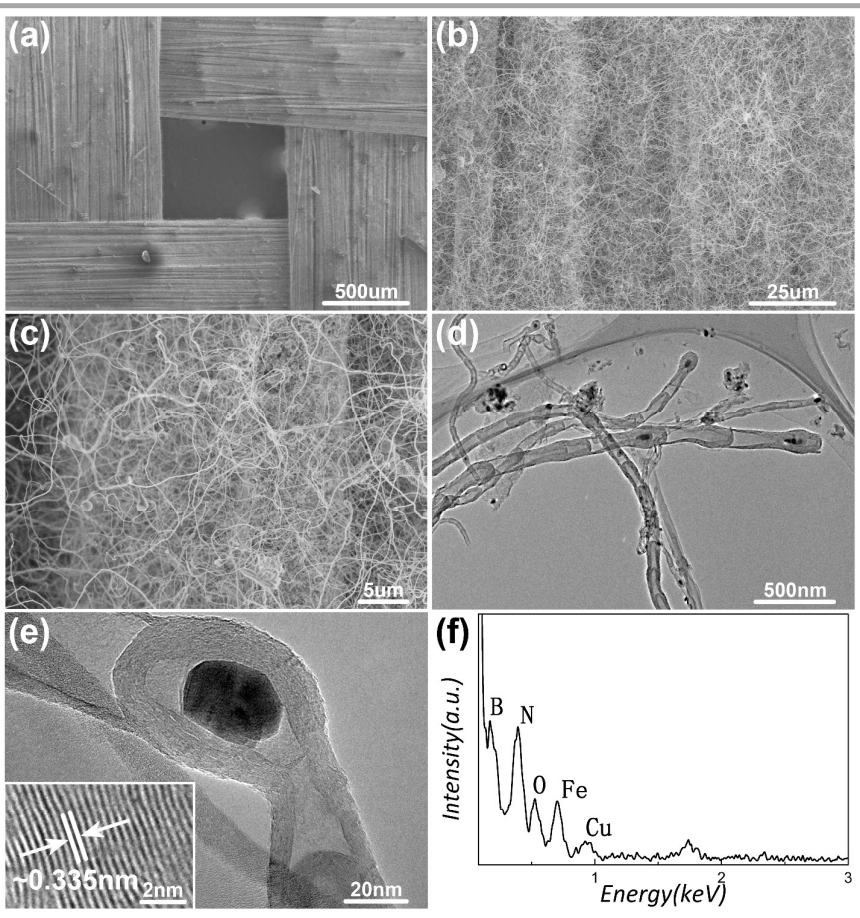


**Fig. 1** (a-c) Low-magnification SEM images of BNNTs in situ grown on fiber cloth. (d) and (e) TEM images of bamboo-like BNNTs. The inset shows the parallel fringes of nanotubes, between which the spacing is ~0.335nm, as labeled in the inset. (f) EDS spectra of BNNTs. The strong B and N peaks confirm that the nanotubes are BNNTs. The Fe element is attributable to the steel particles introduced by ball-milling treatment with stainless steel balls. The Cu peak derives from the Cu TEM grid and O element may be ascribed to the surrounding air absorbed on the surface of nanotubes.

After densification by CVI and PIP methods,  $SiC_f/SiC$  composites and  $SiC_f/BNNTs$ -SiC hierarchical composites with about 1 wt% BNNTs in situ grown were obtained. The density, open porosity, flexural strength and fracture toughness of these two kinds of composites were measured and given in Table 1. It can be seen that  $SiC_f/BNNTs$ -SiC hierarchical composites have an average density of  $2.58\pm0.04~g.cm^{-3}$  and an open porosity of  $5.11\pm1.30~\%$  while  $2.69\pm0.03~g.cm^{-3}$  and

4.22 $\pm$ 1.12 % for SiC<sub>f</sub>/SiC composites. This result implies that the incorporation of BNNTs into SiC<sub>f</sub>/SiC composites gives rise to a decline in average density of the composites and correspondingly an increase in open porosity. This phenomenon is also affirmed by the observation of the polished cross-sections of the composites, as exhibited in Fig. 2. In Fig. 2a, several relatively small intra-bundle pores are observed in the fiber bundle of SiC<sub>f</sub>/SiC composites resulting

 $\textbf{Table 1} \ \text{Properties of SiC}_{\text{f}}/\text{SiC composites and SiC}_{\text{f}}/\text{BNNTs-SiC hierarchical composites}.$ 

Composites	BNNTs content (wt%)	Density (g.cm <sup>-3</sup> )	Open porosity (%)	Flexural strength (MPa)	Fracture toughness (MPam <sup>1/2</sup> )
SiC <sub>f</sub> /SiC	0	2.69±0.03	4.22±1.12	482.9±45.6	15.5±2.8
SiC <sub>f</sub> /BNNTs-SiC	1.0	2.58±0.04	5.11±1.30	442.7±24.8	15.3±1.0

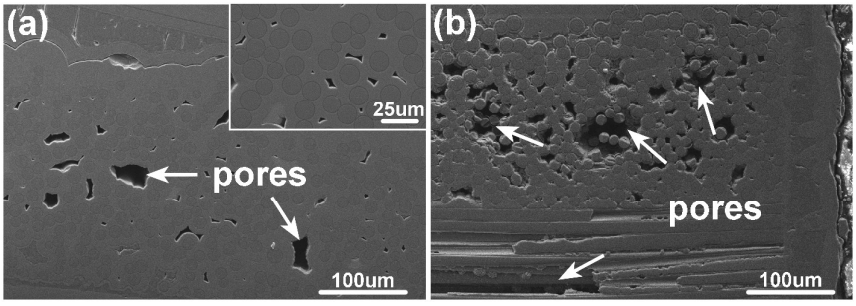


Fig. 2 Low-magnification SEM images of the polished cross-sections of the fiber bundle in (a)  $SiC_f/SiC$  composites and (b)  $SiC_f/BNNTs-SiC$  hierarchical composites. Pores are observed in both two composites, as indicated by white arrows. The inset shows the enlarged image of the polished cross-section of the fiber bundle in  $SiC_f/SiC$  composites.

from the stop of matrix densification when the surface pores are closed, which is inevitable and an intrinsic flaw of CVI method.<sup>18</sup> However, in this case, although intra-bundle pores exist, all the fibers are deposited with matrix with the thickness of at least about 3um, which can be seen in the inset in Fig. 2a. So the SiC<sub>f</sub>/SiC composites are relatively dense with a lower open porosity compared with the SiC<sub>f</sub>/BNNTs-SiC hierarchical composites. On the contrary, in the SiC<sub>f</sub>/BNNTs-SiC hierarchical composites, much more and larger intra-bundle pores are observed in the fiber bundle, as shown in Fig. 2b. What's worse, almost all the fibers in the center region of fiber bundle fail to be deposited with matrix and only the fibers close to the surface of fiber bundle are densified with matrix. This phenomenon results in a lower density of the SiC<sub>f</sub>/BNNTs-SiC hierarchical composites, which also bothers Manocha et al. 19 in SiC/C composites incorporated with CNTs. Considering that the two kinds of composites are fabricated under the same condition with the same fiber fabric, the only possible reason for this different densification is the introduction of BNNTs in situ grown on the surface of fibers into SiC<sub>f</sub>/BNNTs-SiC hierarchical composites. The existence of BNNTs divides the micro-scale pores into nanoscale ones among fibers. During CVI process, the nanoscale pores diminish quickly and can be sealed easily, resulting in an earlier clogging of the pore channels in the surface region of fiber bundle and therefore leading to an improper infiltration of matrix in the center

region.<sup>20</sup> In other words, to some extent, BNNTs in situ grown in the surface region of fiber bundle exacerbate the intrinsic downside of CVI method as mentioned above. Such large intrabundle pores unfilled with enough matrix as structural defects in SiC<sub>f</sub>/BNNTs-SiC hierarchical composites definitely will pose stress concentration in the matrix and undermine the effective load transfer from matrix to fibers. They also will impair the positive interfacial friction between matrix and fibers during the fiber pullout. So eventually these structural defects will give rise to the great decrease of mechanical properties including strength and toughness. It is in consistence with the reported results about declined strength of polymer, ceramic or carbon/carbon composites reinforced by BNNTs or CNTs, 21which is also ascribed to the lower density and higher porosity in the composites incorporated with nanotubes. Nevertheless, by comparing mechanical properties of two kinds of composites, as listed in Table 1, it can be noticed that SiC<sub>f</sub>/BNNTs-SiC hierarchical composites have an average flexural strength of 442.7±24.8 MPa, which is only slightly lower than that of 482.9±45.6 MPa for SiC<sub>f</sub>/SiC composites. What's more, the average fracture toughness of SiC<sub>f</sub>/BNNTs-SiC hierarchical composites is 15.3±1.0 MPam<sup>1/2</sup>, which is almost equivalent to that of 15.5±2.8 MPam<sup>1/2</sup> for SiC<sub>f</sub>/SiC composites. This result as discussed above hints that the incorporation of BNNTs into SiC<sub>f</sub>/SiC composites indeed yields

a positive effect on the mechanical properties of the composites.

To identify the evidence about positive effect of BNNTs on mechanical properties of the composites, morphologies of the polished cross-sections and fracture surfaces of SiC<sub>f</sub>/BNNTs-SiC hierarchical composites were investigated via FESEM, as displayed in Fig. 3 and 4. Fig. 3a and b show the low-magnification SEM images of the polished cross-sections of

SiC<sub>f</sub>/BNNTs-SiC hierarchical composites. It can be found that space among horizontal and vertical fibers is not fully densified with matrix, which is in line with the low density of composites as discussed before. In these areas with an insufficiently deposited matrix, many apparent micro-scale rods can be readily observed. The high-magnification SEM image of microscale rods (Fig. 3c) reveals that such micro-scale rods twine with each other with the diameters of 0.8-1um. These microscale rods are believed to develop from the original nanotubes

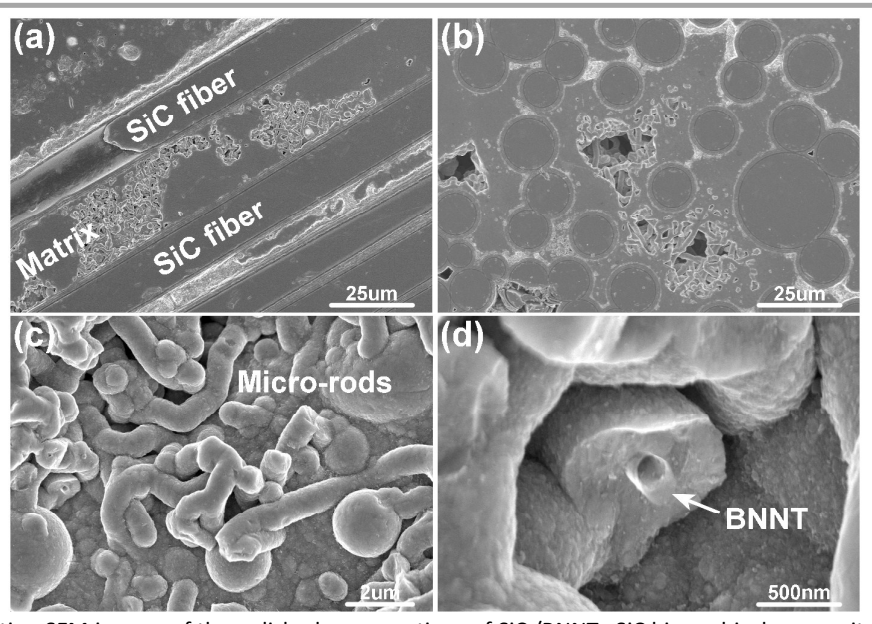


**Fig. 3** Low-magnification SEM images of the polished cross-sections of SiC<sub>f</sub>/BNNTs-SiC hierarchical composites: (a) horizontal and (b) vertical fibers. High-magnification SEM images of micro-scale rods in the areas with an insufficiently deposited matrix, showing (c) the overall morphology of micro-scale rods and (d) a broken micro-scale rod with a BNNT inside.

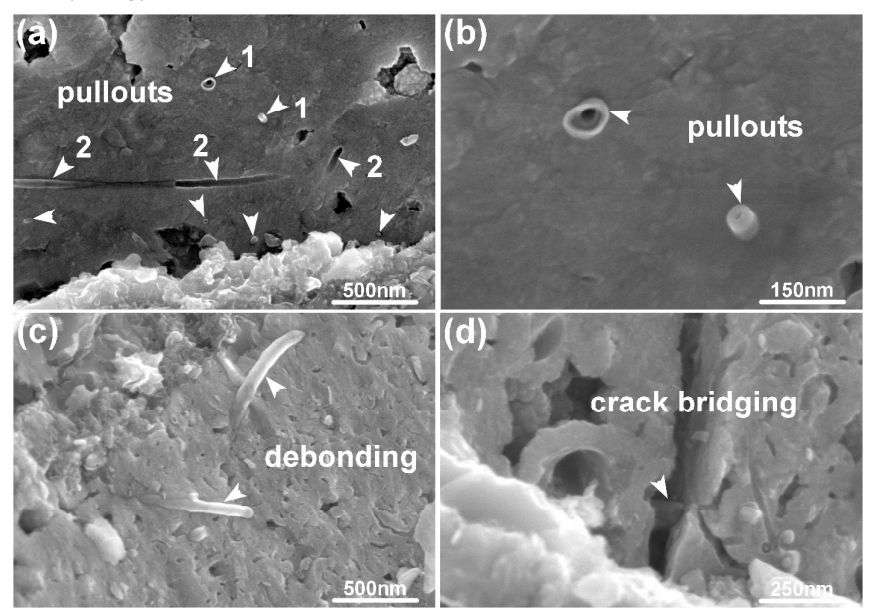


**Fig. 4** High-magnification SEM images of the fracture surfaces of matrix among fibers in  $SiC_f$ /BNNTs-SiC hierarchical composites, showing typical morphology of (a) and (b) the pullouts of BNNTs, (c) debonding between BNNTs and matrix and (d) crack bridging by BNNTs.

after the subsequent CVI matrix densification process. During the CVI process, matrix is deposited on the surface of nanotubes, but fails to be dense. It can be confirmed from a broken micro-scale rod as shown in Fig.3d, which clearly displays that there is a BNNT inside the micro-scale rod. The above result also demonstrates that BNNTs were successfully introduced into the matrix among fibers. The morphology of the fracture surfaces of matrix among fibers in SiC<sub>f</sub>/BNNTs-SiC hierarchical composites was exhibited in Fig. 4. It can be clearly seen that BNNTs pull out from matrix, leading to some pores or slots left in the matrix, as shown in Fig. 4a and b. Fig. 4c apparently indicates that the interfacial debonding between BNNTs and matrix occurs in the fracture surface. In addition, it is believed that crack deflection definitely also happens during above mentioned pullout and debonding.<sup>25</sup> Moreover, from Fig. 4d, it also can be observed that crack is bridged by a BNNT with its ends firmly embedded in matrix. It is universally acknowledged that pullout, debonding, crack deflection and crack bridging are the major strengthening and toughening mechanisms for micro-scale fibers reinforced composites. In our work, such strengthening and toughening mechanisms are observed as well in the matrix of SiC<sub>f</sub>/SiC composites incorporated with BNNTs, which are aroused by nanoscale reinforcements of BNNTs. When the propagating crack encounters BNNTs vertical to the propagation direction or with a certain angle (indicated in Fig. 4 a by arrow 1 and 2, respectively), the crack is deflected and BNNTs are stretched across the crack, exhibiting the phenomenon of crack bridging as shown in Fig. 4d. BNNTs will break when reaching their critical strain or pull out when reaching the interfacial bonding strength. These processes will dissipate some fracture energy.<sup>22</sup> In addition, BNNTs parallel to the propagation direction of crack also deflect the crack and are peeled away from the matrix after the interfacial debonding, as displayed in Fig. 4c, which also absorbs some energy.<sup>26</sup> These abovediscussed energy dissipation mechanisms at nanoscale triggered by BNNTs spotlights the evidence that the incorporation of BNNTs into SiC<sub>f</sub>/SiC composites is propitious for improving mechanical properties of the composites. Merely, the real contribution of BNNTs to mechanical properties of the composites may be partially offset by the negative effect of the low density and high porosity. It suggests that careful consideration is needed for the densification of hierarchical composites in our further study to avoid above flaw. There are two possible ways to reduce the porosity of the hierarchical composites. The first one is to slow down the deposition rate of SiC matrix during the CVI process by decreasing the deposition pressure (i.e. the concentration of precursors in the CVI furnace) or temperature so that the nanoscale pore channels in the surface region of fiber bundle will not be clogged too early. In this case, more time for the matrix deposition in the center region of fiber bundle is obtained. This method is a widely-used way to relieve the above-mentioned intrinsic flaw of CVI process. The other approach to increase the density and decrease the porosity of hierarchical composites is using impregnation/pyrolysis (PIP) method to introduce SiC matrix into the center region of fiber bundle. The PIP method used in this paper is only for the densification of some relatively large pores among fiber bundles, as mentioned in the experimental section. When it is adopted for the densification of the center region of fiber bundle, the capillary force from the nanoscale pores channels will be beneficial for the polymer precursor infiltration into the fiber bundle, thus being good for reducing the porosity.

On the other hand, as exhibited in Fig. 4b, the pullouts of BNNTs vertical to the fracture surface are very short, which may limit the toughening effect arising from the interfacial friction during the pullout. According to the results reported by Wang et al. 26 and Tatarko et al., 27 a rather strong interface bonding, which originates from chemical reaction between matrix and the reinforcement phase, may be responsible for the short pullout length. However, given that BNNTs are chemically stable and the surfaces of BNNTs pulling out or debonding from matrix (as indicated in Fig. 4a and c, respectively) are very smooth without adhered matrix, this explanation can't hold water for our study. In fact, as discussed before about the microstructure of BNNTs, almost all the BNNTs have the bubble-chain walls with obvious periodical knots. These knots can act as structural anchors and cause mechanical interlocking between the matrix and BNNTs, thus resulting in strong interface bonding and short pullout length. It also has been found in ceramic or mental reinforced by bamboo-like CNTs or SiC nanowires with obvious knots. 28,29 Additionally, unlike cylindrical nanotubes, bamboo-like BNNTs prefer to break at the inner joints due to the discontinuity of the lattice, <sup>27,30</sup> as affirmed in Fig. 4b, which also brings about short pullout length.

To evaluate the oxidation resistance of SiC<sub>f</sub>/SiC composites and SiC<sub>f</sub>/BNNTs-SiC hierarchical composites, static oxidation test was conducted at 900°C for 40 h. Fig. 5a and b show the overall morphologies of the polished cross-sections of the composites after oxidation. By comparison with that before oxidation as displayed in Fig. 2, it can be found that after oxidation fibers and intra-bundle matrix of SiC<sub>f</sub>/SiC composites seem to be fragmented. Clear comparisons about highmagnification SEM images of the fiber bundle in SiC<sub>f</sub>/SiC composites before and after static oxidation are exhibited in Fig. 5c-f. Before oxidation, the polished cross-section is smooth and multilayered interphases (PyC/SiC)<sub>n</sub> (n=3) are intact, as shown in Fig. 5c and e. After oxidation, it can be seen from Fig. 5d that the polished cross-section is bumpy and a lot of annular slots appear circumferential to fibers in SiC<sub>f</sub>/SiC composites. Fig. 5f obviously reveals that these slots arise from the disappearance of oxidized PyC interphase. However, by contrast, no significant distinction about the overall morphology of the polished cross-sections of SiC<sub>f</sub>/BNNTs-SiC hierarchical composites before and after oxidation can be observed from Fig. 2b and Fig. 5b. Only PyC interphase close to the crack that is the diffusion channel of oxygen into fiber bundles is oxidized and multilayered interphases are partly broken, as indicated by white arrows in the inset in Fig. 5b. The

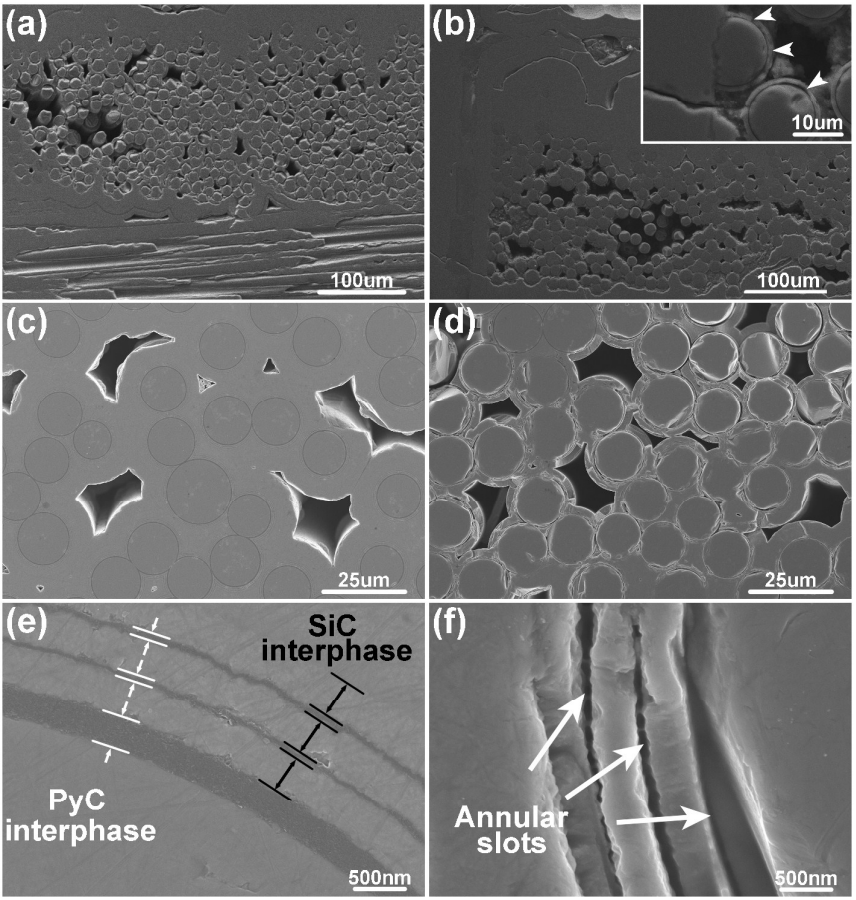


Fig. 5 Low-magnification SEM images of the polished cross-sections of (a)  $SiC_f/SiC$  composites and (b)  $SiC_f/BNNTs-SiC$  hierarchical composites after static oxidation at  $900^{\circ}C$  for 40h. The enlarged view of fibers near the crack is inserted in the right image. High-magnification SEM images of the fiber bundle in  $SiC_f/SiC$  composites: (b) and (d) before and (c) and (e) after oxidation.

above result infers that SiC<sub>f</sub>/BNNTs-SiC hierarchical composites have a better oxidation resistance than SiC<sub>f</sub>/SiC composites. To pin down the oxidation kinetics of the composites, the weight losses of composites as a function of oxidation time were recorded. From the experimental data (square dots) and corresponding fitting curves (red lines) of the weight losses of composites as depicted in Fig. 6, it can be seen that the weight loss of SiC<sub>f</sub>/SiC composites increases linearly with respect to the oxidation time while that of SiC<sub>f</sub>/BNNTs-SiC hierarchical composites exhibits a parabolic behavior. As discussed above, the disappearance of oxidized PyC interphase is responsible for the weight losses of composites. In this paper, it can be estimated that PyC interphase accounts for about 2.5 wt% of the composites. After oxidation at 900°C for 40h, the weight loss of SiC<sub>f</sub>/SiC composites reaches 0.47 wt% while that of SiCf/BNNTs-SiC hierarchical composites is only 0.37 wt%. The PyC interphase is oxidized above  $400^{\circ}$ C, of which the key steps are given as follows: (1) Diffusion of oxygen to PyC interphase. (2) Chemical reaction between oxygen and PyC interphase. (3) Diffusion of the products CO and/or CO2 away from PyC interphase.31 The oxidation behavior of PyC interphase in

 $SiC_f/SiC$  composites can be described by linear-parabolic kinetics:  $^{32}$ 

$$x^2/k_p + x/k_1 = t ag{3}$$

where x is the recession distance, t is the oxidation time,  $k_{\scriptscriptstyle D}$  is the parabolic rate constant and  $k_1$  is the linear rate constant. In eqn(3), the first part is related to the diffusion of oxygen and the second one is concerned with the carbon and oxygen reaction. When the diffusion of oxygen to PyC interphase is very easy through the cracks or pores, the interior has a high concentration of oxygen and the oxidation reaction is nearly uniform. Namely, in this case  $k_p$  is higher than  $k_1$  and the first part can be ignored. 32,33 The oxidation of PyC interphase is a reaction-controlled process and corresponds to linear kinetics, as shown in Fig. 6a. On the contrary, when the diffusion of oxygen is hindered, there is a starvation for oxygen in the interior and the oxidation reaction only occurs near the outside surface where oxygen is abundant. So  $k_{\scriptscriptstyle D}$  is smaller than  $k_1$  and the oxidation of PyC interphase is a diffusioncontrolled process, exhibiting a parabolic behavior, as affirmed in Fig. 6b. From above discussion, it can be demonstrated that the diffusion of oxygen in SiC<sub>f</sub>/BNNTs-SiC hierarchical composites is blocked to a great extent. Additionally, it needs

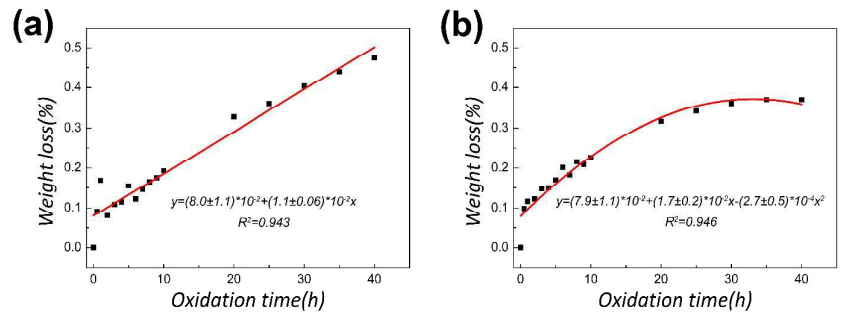


**Fig. 6** Weight losses of (a) SiC<sub>f</sub>/SiC composites and (b) SiC<sub>f</sub>/BNNTs-SiC hierarchical composites as a function of time oxidized in static air at  $900^{\circ}$ C for 40h: experimental data (square dots) and fitting curves (red lines). The curve-fitting equations and corresponding coefficients of determination (R<sup>2</sup>) are given in the figures.

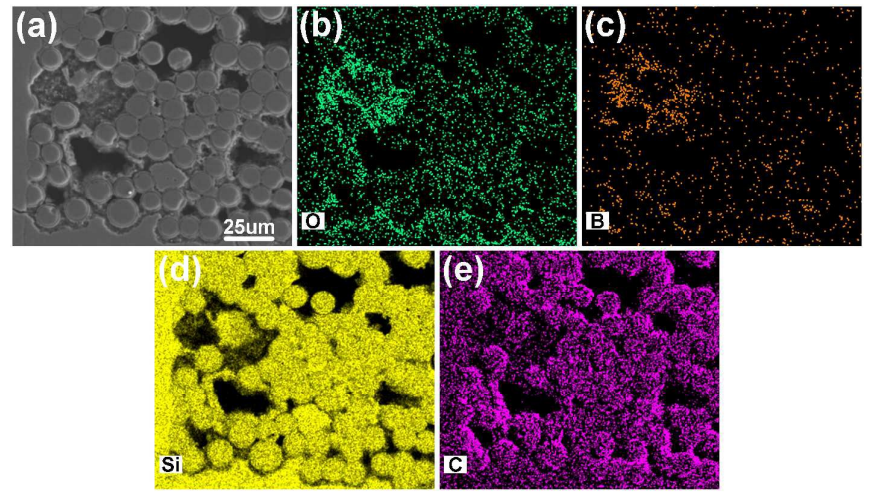
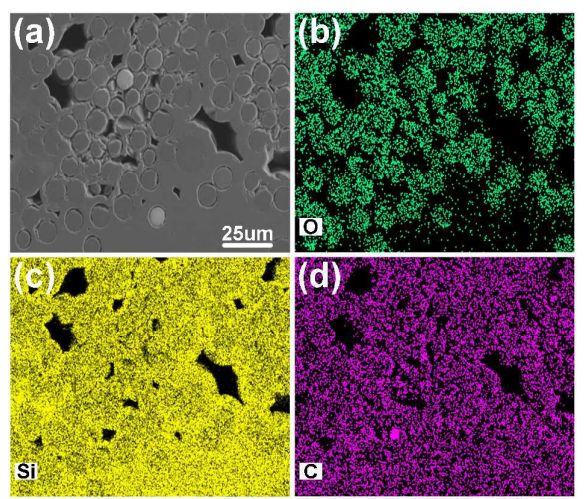


Fig. 7 (a) SEM image of the polished cross-section of  $SiC_f/BNNTs$ -SiC hierarchical composites after oxidation, along with corresponding (b-e) EDS elemental mapping images of O, B, Si and C. O element aggregation is observed in the area where B element is located.



**Fig. 8** (a) SEM image of the polished cross-section of SiC<sub>f</sub>/SiC composites after oxidation, along with corresponding (b-d) EDS elemental mapping images of O, Si and C. O element is mainly distributed in the fibers.

to be especially clarified that the above explanation is based on the assumption that the oxidation of SiC at  $900^{\circ}$ C can be neglected due to its low passive oxidation rate. <sup>32,34</sup> However,

in fact it can't be ignored especially when long oxidation time such as several tens of hours is concerned.<sup>35-37</sup> The formation of silica from the passive oxidation of SiC can result in the

weight gain of composites and narrow the cracks, thus giving rise to a decreasing weight loss and a tendency of transition of oxidation behavior from linear to parabolic kinetics. A slight sign of this phenomenon can be observed from experimental data in Fig. 6a. But the influence of this phenomenon is limited

because the amount of silica is relatively small and the cracks are not completely but slightly narrowed.  $^{34,38,39}$  Hence, extremely clear parabolic oxidation kinetics of SiC<sub>f</sub>/BNNTs-SiC hierarchical composites should be attributed to some other mechanisms.

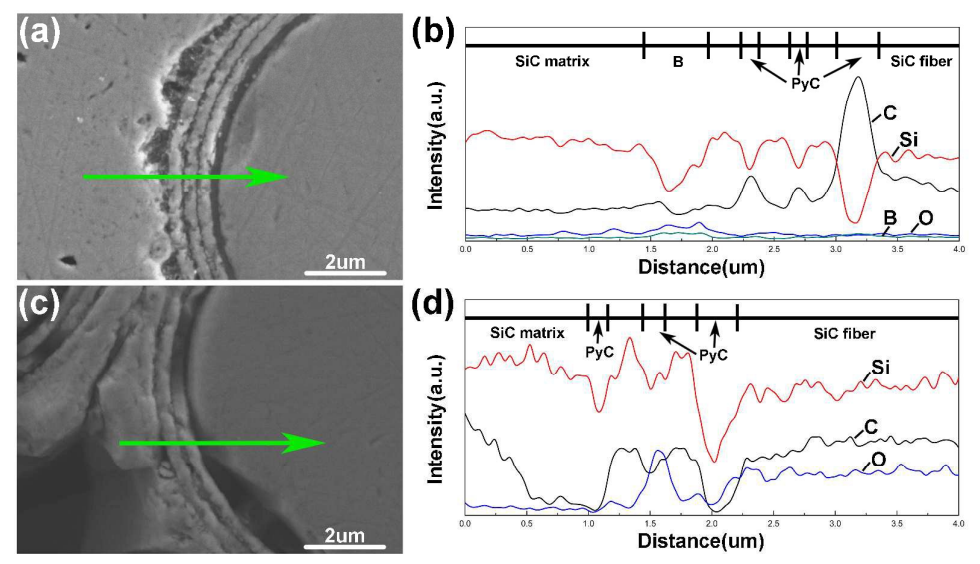


Fig. 9 EDS elemental line scan profiles of the polished cross-sections of (a) and (b)  $SiC_f/BNNTs-SiC$  hierarchical composites and (c) and (d)  $SiC_f/SiC$  composites after oxidation. The positions of SiC matrix, multilayered interphases (PyC/SiC)<sub>n</sub> (n=3), boron powder and SiC fiber before oxidation are depicted in the two images on the right.

To develop a comprehensive understanding of the mechanism of oxidation resistance, the distributions of different elements in the fiber bundle after oxidation were investigated by EDS. Fig. 7 and Fig. 8 show the SEM images of the polished cross-sections of SiC<sub>f</sub>/BNNTs-SiC hierarchical composites and SiC<sub>f</sub>/SiC composites after oxidation, along with corresponding EDS elemental mapping images of O, B, Si and C. The Si and C elemental mapping images are in good agreement with the distributions of SiC matrix and fibers in both composites. Additionally, it can be seen from Fig. 7e that the concentration of C element circumferential to fibers in SiC<sub>f</sub>/BNNTs-SiC hierarchical composites is relatively high, which is hardly found in SiC<sub>f</sub>/SiC composites from Fig. 8d. Such relatively high concentration of C element is ascribed to the PyC interphase surviving after oxidation. Moreover, as shown in Fig. 7b and c, O element aggregation is observed near the outside surface of the fiber bundle, especially in the area where B element is located, inferring that the glassy phase (B2O3) is produced by the reaction of oxygen and boron powder in such area. <sup>2,16</sup> This glassy phase has a low viscosity at 900°C and can seal the diffusion channel of oxygen further into the fiber bundle in some degree. 16 So the concentration of O element in the interior of the fiber bundle is relatively low. By contrast, in SiC<sub>f</sub>/SiC composites O element diffuses into the fiber bundle very easily, thus inducing the oxidation of the PyC interphase and even the fibers. Consequently, oxygen is mainly distributed in the fibers as exhibited in Fig. 8b. In fact, SiC fibers cannot be oxidized completely because of their low passive oxidation rate at 900°C. So precisely speaking, O

element diffusing from the exterior should be distributed in the silica layer at the edges of fibers. O element in the center of the fiber is regarded as an inevitable impurity element that as-received SiC fibers often contain. Further investigation on the distributions of different elements from the matrix to the fiber after oxidation were also conducted by EDS. Fig. 9 shows EDS elemental line scan profiles of the polished cross-sections of SiC<sub>f</sub>/BNNTs-SiC hierarchical composites and SiC<sub>f</sub>/SiC composites after oxidation. Apparently, it can be noticed from Fig. 9a and b that in SiC<sub>f</sub>/BNNTs-SiC hierarchical composites O element is mainly distributed outside the multilayered interphases (PyC/SiC)<sub>n</sub> (n=3) where the residual boron powder is situated. It implies that oxygen is blocked outside the multilayered interphases and the fiber by the oxidation of the residual boron powder, from which the glassy phase (B2O3) with a low viscosity can seal the diffusion channel of oxygen. Hence, from the multilayered interphases to the fiber, almost no oxygen can be found. The PyC interphase succeeds to survive after oxidation for 40h at 900°C, as affirmed by the three peaks of C concentration curve in Fig. 9b corresponding to three layers of PyC interphases. On the contrary, O element is detected in the multilayered interphases and even the fiber in SiC<sub>f</sub>/SiC composites, as revealed in Fig. 9c and d. At the positions where three layers of PyC interphases are located, no peaks of C concentration curve can be observed. Moreover, the concentration of O element in the fiber is obviously higher than that in the matrix, which is not observed in SiC<sub>f</sub>/BNNTs-SiC hierarchical composites (Fig. 9b). It gives the evidence that because of no obstruction to the diffusion of oxygen towards

the multilayered interphases, the PyC interphase is easily oxidized and even eventually O element also diffuses into the fiber. The above analysis of EDS results demonstrates that the anticipation that after the growth of BNNTs the residual boron powder besieging the multilayered interphases can hinder the in-depth diffusion of oxygen towards the PyC interphases by oxidizing to form glassy phase  $(B_2O_3)$  is realized, which is considered to be responsible for better oxidation resistance and parabolic oxidation kinetics of  $SiC_f/BNNTs$ -SiC hierarchical composites at  $900\,^{\circ}\mathrm{C}$  for 40h.

**Table 2** Flexural strength and strength retention of  $SiC_f/SiC$  composites and  $SiC_f/BNNTs-SiC$  hierarchical composites before and after oxidation in static air at  $900^{\circ}C$  for 40h.

Composit	BNNTs content (wt%)	Flexural str	Strength	
es		Before oxidation	After oxidation	retention (%)
SiC <sub>f</sub> /SiC	0	482.9±45.	424.4±50.4	87.8
SiC <sub>f</sub> /BNN Ts-SiC	1.0	442.7±24. 8	419.1±34.0	94.7

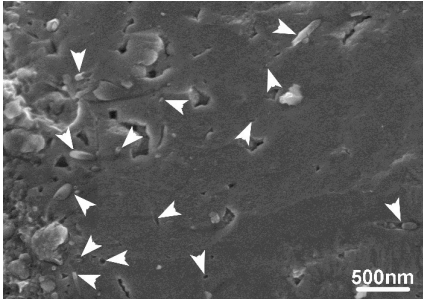


**Fig. 10** High-magnification SEM image of the fracture surface of matrix among fibers in SiC<sub>f</sub>/BNNTs-SiC hierarchical composites after oxidation, showing typical morphology of the pullouts of BNNTs.

The flexural strength and strength retention of SiC<sub>f</sub>/SiC composites and SiC<sub>f</sub>/BNNTs-SiC hierarchical composites after oxidation in static air at 900°C for 40h were also evaluated and summarized in Table 2. After oxidation, the flexural strength of SiC<sub>f</sub>/BNNTs-SiC hierarchical composites declines 442.7±24.8 MPa to 419.1±34.0 MPa while from 482.9±45.6 MPa to 424.4±50.4 MPa for SiC<sub>f</sub>/SiC composites. By comparing the strength retentions of two composites, it can be found that after oxidation SiC<sub>f</sub>/BNNTs-SiC hierarchical composites can retain 94.7% of the initial flexural strength while only 87.8% for SiC<sub>f</sub>/SiC composites. No doubt that it is the direct reflection of improved oxidation resistance of SiC<sub>f</sub>/BNNTs-SiC hierarchical composites thanks to the residual boron powder that ensures that little PyC interphase is oxidized for 40h at 900°C. Fig. 10 shows the morphology of the fracture surface of matrix among fibers in SiC<sub>f</sub>/BNNTs-SiC hierarchical composites after oxidation. The pullouts of BNNTs clearly can be seen in the matrix, as indicated by white arrows in Fig. 10. It infers that BNNTs in composites succeed to survive after oxidation and

still can play a role as nanoscale reinforcements to bring about strengthening and toughening mechanisms at nanoscale in  $SiC_f/BNNTs$ -SiC hierarchical composites. So it is believed that the surviving BNNTs in composites probably also make a contribution to the better strength retention after oxidation.

#### **Conclusions**

SiC<sub>f</sub>/BNNTs-SiC hierarchical composites were fabricated via firstly in situ growth of BNNTs on the surface of SiC fibers and subsequently matrix densification via CVI and PIP methods. The as-grown BNNTs utterly encompass the fiber cloth and exhibit a multi-walled and bamboo-like structure with an average diameter of 30-160nm and a length of several tens of micrometers. In addition, almost all the BNNTs apparently possess the bubble-chain walls. BNNTs in SiC<sub>f</sub>/SiC composites divide the micro-scale pores into nanoscale ones among fibers. Due to an earlier clogging of these nanoscale pore channels and thus an improper infiltration of matrix during CVI process, the incorporation of BNNTs into SiC<sub>f</sub>/SiC composites gives rise to a decline in density of composites and correspondingly an increase in open porosity. However, even with these insufficient filled pores as structural defects, flexural strength of the SiC<sub>f</sub>/BNNTs-SiC hierarchical composites is only slightly undermined while fracture toughness displays almost no decrease. Pullout, debonding, crack deflection and crack bridging attributed to BNNTs are observed, which are considered as energy dissipation mechanisms at nanoscale triggered by nanoscale reinforcements. It verifies the positive effect of BNNTs on the mechanical properties of the composites. Additionally, SiC<sub>f</sub>/BNNTs-SiC hierarchical composites achieve an improved oxidation resistance and parabolic oxidation kinetics at 900°C for 40h. It is attributable to the mechanism that after the growth of BNNTs the residual boron powder besieging the multilayered interphases can hinder the in-depth diffusion of oxygen towards the PyC interphases by oxidizing to form glassy phase (B<sub>2</sub>O<sub>3</sub>). Moreover, SiC<sub>f</sub>/BNNTs-SiC hierarchical composites possess a better strength retention after oxidation. This is believed to not only be the direct reflection of improved oxidation resistance thanks to the residual boron powder but also benefit from the remained strengthening and toughening mechanisms aroused by BNNTs surviving after oxidation.

#### Acknowledgements

This work is supported by the National Natural Science Foundation of China (Grant No. 51502323 and 51172256), Shanghai Key Project of Basic Research (Grant No. 14JC1406200) and Shanghai Scientific Research Project (Grant No. 13521101203).

#### Notes and references

1 S. Schmidt, S. Beyer, H. Knabe, H. Immich, R. Meistring, A. Gessler, *Acta Astronaut.*, 2004, **55**, 409-420.

- 2 R. Naslain, Compos. Sci. Technol., 2004, 64, 155-170.
- 3 W. Krenkel, Ceramic matrix composites: fiber reinforced ceramics and their applications, Wiley-VCH, Weinheim, 2008.
- 4 J. Hu, S. Dong, X. Zhang, H. Zhou, B. Wu, Z Wang, et al, Composites Part A, 2013, 48, 73-81.
- H. Qian, E. S. Greenhalgh, M. S. Shaffer, A. Bismarck, J. Mater. Chem., 2010, 20, 4751-4762.
- 6 A. Godara, L. Mezzo, F. Luizi, A. Warrier, S. V. Lomov, A. W. Van Vuure, et al, *Carbon*, 2009, **47**, 2914-2923.
- 7 J. Hu, S. Dong, Q. Feng, M. Zhou, X Wang, Y Cheng, *Carbon*, 2014. **69**. 621-625.
- A. Y. Boroujeni, M. Tehrani, A. J. Nelson, M. Al-Haik, *Composites Part B*, 2014, 66, 475-483.
- 9 E. Bekyarova, E. T. Thostenson, A. Yu, H. Kim, J. Gao, J. Tang, et al, *Langmuir*, 2007, 23, 3970-3974.
- 10 Y. Chen, J. Zou, S. J. Campbell, G. Le Caer, *Appl. Phys. Lett.*, 2004, **84**, 2430-2432.
- 11 C. Zhi, Y. Bando, C. Tang, D. Golberg, Mater. Sci. Eng., R, 2010, 70, 92-111.
- 2010, **70**, 92-111. 12 A. Pakdel, C. Zhi, Y. Bando, D. Golberg, *Mater. Today*, 2010,
- 15, 256-265.13 C. Y. Zhi, Y. Bando, C. C. Tang, Q. Huang, D. Golberg, J. Mater.
- Chem., 2008, **18**, 3900-3908.
- 14 M. Schulz, V. Shanov, Z. Yin, Nanotube Superfiber Materials: Changing Engineering Design, William Andrew, New York, 2013.
- 15 G. Zhu, S. Dong, J. Hu, Y. Kan, P. He, L. Gao, et al, *RSC Adv.*, 2016, **6**, 14112-14119.
- 16 R. Naslain, A. Guette, F. Rebillat, R. Pailler, F. Langlais, X. Bourrat, J. Solid State Chem., 2004, 177, 449-456.
- 17 M. Du, J. Q. Bi, W. L. Wang, X. L. Sun, N. N. Long, *Mater. Sci. Eng.*, A, 2012, **543**, 271-276.
- 18 W. Feng, L. Zhang, Y. Liu, X. Li, L. Cheng, B. Chen, *Mater. Sci. Eng.*, A, 2015, 626, 500-504.
- 19 L. M. Manocha, R. Pande, J. Nanosci. Nanotechnol., 2010, 10, 3822-3827.
- W. J. Kim, S. M. Kang, J. Y. Park, W. S. Ryu, Fusion Eng. Des., 2006. 81, 931-936.
- 21 C. Y. Zhi, Y. Bando, W. L. Wang, C. C. Tang, H. Kuwahara, D. Golberg, J. Nanomater., 2008, 2008.
- 22 Y. F. Chen, J. Q. Bi, W. L. Wang, Y. Zhao, G. L. You, C. L. Yin, et al, *Mater. Sci. Eng.*, A, 2014, **590**, 16-20.
- 23 A. Peigney, Nat. Mater., 2003, 2, 15-16.
- 24 H. Zhang, L. Guo, Q. Song, Q. Fu, H. Li, K. Li, *Prog. Nat. Sci.*, 2013, **23**, 157-163.
- 25 H. H. Yu, S. R. Wang, L. Y. Yang, Appl. Compos. Mater., 2013, 20, 947-960.
- 26 W. L. Wang, J. Q. Bi, S. R. Wang, K. N. Sun, M. Du, N. N. Long, et al, J. Eur. Ceram. Soc., 2011, 31, 2277-2284.
- 27 P. Tatarko, S. Grasso, H. Porwal, Z. Chlup, R. Saggar, I. Dlouhý, et al, J. Eur. Ceram. Soc., 2014, 34, 3339-3349.
- 28 M. Olek, J. Ostrander, S. Jurga, H. Möhwald, N. Kotov, K. Kempa, et al, *Nano Lett.*, 2004, 4, 1889-1895.
- 29 Y. Chu, H. Li, Y. Wang, L. Qi, Q. Fu, Surf. Coat. Technol., 2013, 235, 577-581.
- 30 D. M. Tang, C. L. Ren, X. Wei, M. S. Wang, C. Liu, Y. Bando, et al, ACS Nano, 2011, 5, 7362-7368.
- 31 N. Jacobson, D. Hull, J. Cawley, D. Curry, Kinetics and mechanism of oxidation of the reinforced carbon/carbon on the space shuttle orbiter, Proceedings of 34th international conference and exposition on Advanced Ceramics and Composites, 2010, 3-21.
- 32 A. J. Eckel, J. D. Cawley, T. A. Parthasarathy, *J. Am. Ceram. Soc.*, 1995, **78**, 972-980.
- 33 J. D. Cawley, E. Ave, W. Bld, Modeling the oxidation kinetics of continuous carbon fibers in a ceramic matrix, Proceedings of 23nd Annual Conference on Composites, Advanced

- Ceramics, Materials, and Structures-B: Ceramic Engineering and Science Proceedings, 1999, 87.
- 34 Y. Xu, W. Zhang, Numerical simulation of oxidation-assisted failure of CMC-SiC at intermediate temperature, Proceedings of 8th High Temperature Ceramic Matrix Composites Conference: Ceramic Transactions, 2013, 65-76.
- 35 R. H. Jones, C. H. Henager, C. A. Lewinsohn, C. F. Windisch, *J. Am. Ceram. Soc.*, 2000, **83**, 1999-2005.
- 36 I. Sebire-Ihermitte, M. Gomina, J. Vicens, J. Microsc., 1993, 169, 197-205.
- 37 Ö. Ünal, A. J. Eckel, F. C. Laabs, Mechanical properties and microstructure of oxidized SiC/SiC composites, Proceedings of 20th Annual Conference on Composites, Advanced Ceramics, Materials, and Structures-B: Ceramic Engineering and Science Proceedings, 1996, 333-341.
- 38 C. E. Ramberg, G. Cruciani, K. E. Spear, R. E. Tressler, C. F. Ramberg, *J. Am. Ceram. Soc.*, 1996, **79**, 2897-2911.
- 39 L. Filipuzzi, R. Naslain, J. Am. Ceram. Soc., 1994, 77, 467-480.